EUROPEAN ORGANIZATION FOR NUCLEAR RESEARCH

CERN-ATS-2012-066

Revision of Intrabeam Scattering with Non-Ultrarelativistic Corrections and Vertical Dispersion for MAD-X

Fanouria Antoniou and Frank Zimmermann
CERN, Geneva, Switzerland

Abstract

Using the Bjorken-Mtingwa formalism [1] we derive general expressions for the three intrabeam scattering (IBS) growth rates, including non-ultrarelativistic terms and vertical dispersion. These formulae have been implemented (and corrected) in the most recent version of MAD-X. An application to the Large Hadron Collider (LHC) illustrates the effect of crossing angles and detector fields on the vertical IBS growth rate. The IBS growth rates are also calculated for an LHC upgrade optics. A third example, from the damping ring of the Compact Linear Collider (CLIC), demonstrates the importance of the spurious vertical dispersion generated by orbit errors for the vertical IBS growth rate. A model of the Swiss Light Source (SLS) is used as a fourth example to demonstrate the importance of the spurious vertical dispersion for the vertical IBS growth rate in a regime where IBS is weak. Finally, some limitations of this approach to intrabeam scattering are discussed.

This report corrects and supersedes report CERN-AB-2006-002 [2].

Geneva, Switzerland

May 8, 2012

1 Introduction

The motivation for a revision of the MAD-X intrabeam scattering formulae was twofold.

First, CERN experiments at low or medium energy were reported to disagree with the MAD predictions [3]. As a mitigation, Michel Martini recommended the implementation of the Martini-Conte formulae [4], which are a non-ultrarelativistic generalization based on the general Bjorken-Mtingwa formalism [1].

Second, neither the Bjorken-Mtingwa nor the Conte-Martini formulae account for nominal or spurious vertical dispersion, though the latter is thought to make the dominant contribution to the vertical IBS growth rate in many storage rings. Neglecting the vertical dispersion has given rise to peculiar results, such as predicting the shrinkage of the vertical emittance, which are not observed in reality. In linear collider damping rings, intrabeam scattering determines the final vertical emittance and when modeling the damping-ring performance it must properly be accounted for.

In this report we derive extended formulae for the emittance growth due to intrabeam scattering, starting with the general formalism of Bjorken and Mtingwa, and following the approach of Conte and Martini, but including the effect of vertical dispersion. For a number of concrete examples we illustrate that without vertical dispersion the calculated vertical growth intrabeam scattering rate is small and sometimes negative, whereas considering even a tiny amount of vertical dispersion gives a non-negligible positive growth rate. The inclusion of some (e.g. spurious) vertical dispersion also leads to small changes in the computed longitudinal and horizontal growth rates.

Inspection of the original MAD-X code revealed, unexpectedly, that the Conte-Martini formulae [4] were already implemented (presumably they had been copied from the ZAP code [5]), and not the original ones of Bjorken and Mtingwa [1]. We added the terms required for the vertical dispersion.

We note the existence of an alternative formalism of intrabeam scattering, developed earlier by Piwinski [6], as well as of a 'modified' Piwinski formulation proposed by Bane [7], in which D_x^2/β is replaced by the dispersion invariant. Bane has also shown that in the limit of high beam energy the modified Piwinski formalism gives the same results as the Bjorken-Mtingwa one. We have opted for the Bjorken-Mtingwa formalism as basis for calculating intrabeam scattering in MAD-X, since a different variant of this formalism had already been adopted for MAD-8 as well as for an earlier version of MAD-X.

This modified version of MAD-X IBS calculation was first implemented in 2005 and published in 2006 [2]. The published formulae included two mistakes. One was a typo[1], and the other an error in multiplying matrices with Mathematica [9][2]. The actual implementation in MAD-X contained some additional mistakes [3]. This paper presents the correct(ed) expressions and example results obtained with the correct(ed) code.

[1] Two terms, $-2\beta_x/\epsilon_x - \beta_y/\epsilon_y$ were missing in the expression for a_x[8], though correctly included in the code.

[2] This had led to a loss of the terms $6\beta_x^2\phi_x^2/(H_x\epsilon_x)$ and $6\beta_x^2\beta_y\phi_x^2/(H_x\epsilon_x\epsilon_y)$ in the expressions for a_x and b_x, respectively, both in the paper and in the code.

[3] Among other issues, the dispersion in the MAD-X twiss table is defined as $\Delta x/((\Delta\delta)\beta)$ with $\beta = v/c$, which differs from the standard convention for β smaller than 1. We also now distinguish the rms relative energy spread $\Delta E_{\rm rms}/E$ from the rms relative momentum spread, $\delta_{\rm rms}$ according to $\sigma_\delta \equiv \delta_{\rm rms} = (\Delta E_{\rm rms}/E)/\beta^2$.

2 Calculation Approach

The derivation starts with expression (3.4) in [1] for the emittance growth rate in the direction d:

$$\frac{1}{\tau_d} = \frac{\pi^2 r_0^2 c m^3 N(\log)}{\gamma\Gamma} \left\langle \int_0^\infty \frac{d\lambda\ \lambda^{1/2}}{\left[\det\left(L+\lambda I\right)\right]^{1/2}} \left\{ \mathrm{Tr} L^d\ \mathrm{Tr}\left(\frac{1}{L+\lambda I}\right) - 3\ \mathrm{Tr} L^d \left(\frac{1}{L+\lambda I}\right)\right\}\right\rangle , \tag{1}$$

where $d = x$, y, or l, r_0 is the classical particle radius, c the speed of light, m the particle mass, N the number of particles per bunch, $(\log) \equiv \ln\left(r_{\max}/r_{\min}\right)$ a Coulomb logarithm, with $r_{\max}$ denoting the smaller of σ_x and the Debye length and $r_{\min}$ the larger of the classical distance of closest approach and the quantum diffraction limit from the nuclear radius, typically assuming values of $(\log) \approx 15 - 20$, γ the Lorentz factor, and, for a bunched beam, $\Gamma = (2\pi)^3(\beta\gamma)^3 m^3 \epsilon_x \epsilon_y \sigma_\delta \sigma_z$ the 6-dimensional invariant phase space volume of a bunched beam(corrected by a factor of $\sqrt{2}$ [10])[4],

$$L = L^{(x)} + L^{(l)} + L^{(y)} , \tag{2}$$

with

$$L^{(x)} = \frac{\beta_x}{\epsilon_x} \begin{pmatrix} 1 & -\gamma\phi_x & 0 \\ -\gamma\phi_x & \gamma^2 H_x/\beta_x & 0 \\ 0 & 0 & 0 \end{pmatrix} , \tag{3}$$

$$L^{(l)} = \frac{\gamma^2}{\sigma_\delta^2} \begin{pmatrix} 0 & 0 & 0 \\ 0 & 1 & 0 \\ 0 & 0 & 0 \end{pmatrix} , \tag{4}$$

and, generalizing the Bjorken-Mtingwa theory to the case of nonzero vertical dispersion,

$$L^{(y)} = \frac{\beta_y}{\epsilon_y} \begin{pmatrix} 0 & 0 & 0 \\ 0 & \gamma^2 H_y/\beta_y & -\gamma\phi_y \\ 0 & -\gamma\phi_y & 1 \end{pmatrix} . \tag{5}$$

In the above expressions, $\phi_{x,y}$ and $H_{x,y}$ are defined as

$$\phi_{x,y} \equiv D'_{x,y} - \frac{\beta'_{x,y} D_{x,y}}{2\beta_{x,y}} , \tag{6}$$

and

$$H_{x,y} \equiv \frac{D_{x,y}^2 + \beta_{x,y}^2 \phi_{x,y}^2}{\beta_{x,y}} , \tag{7}$$

with $D_{x,y}$ the horizontal or vertical dispersion, $D'_{x,y}$ its slope, $\beta_{x,y}$ the beta function, and $\alpha_{x,y}$ the alpha Twiss function.

Bjorken and Mtingwa [1] proceeded by solving (1) with zero vertical dispersion, and neglecting β_x/ϵ_x and β_y/ϵ_y relative to $(\gamma D_x)^2/(\epsilon_x\beta_x)$, $(\beta_x/\epsilon_x)\gamma^2\phi_x^2$, and γ^2/σ_δ^2. Conte and Martini [4] kept the terms neglected by Bjorken and Mtingwa, which are important for $\gamma < 10$. We also keep these non-ultrarelativistic terms, and, in addition, we include the vertical dispersion.

[4] For an unbunched beam, (1) also applies, if one uses $\Gamma = 4\pi^{5/2}(\beta\gamma)^3 m^3 \epsilon_x \epsilon_y \sigma_\delta C$, with C the ring circumference. In this case, Γ is equal to the 6-dimensional invariant phase space volume divided by $\sqrt{2}$.

3 IBS Growth Rates

For all three cases, namely Bjorken-Mtingwa, Conte-Martini, and the generalized expressions described in this report and now implemented in MAD-X, the three growth rates obtained from (1) can be written in the general form:

$$\begin{aligned}
\frac{1}{\tau_x} &= \frac{\pi^2 r_0^2 v_c m^3 N(\log)}{\gamma\Gamma}\left[\frac{\gamma^2 H_x}{\epsilon_x}\right]\int_0^\infty \frac{d\lambda\ \lambda^{1/2}\left[a_x\lambda + b_x\right]}{(\lambda^3 + a\lambda^2 + b\lambda + c)^{3/2}}\ , \\
\frac{1}{\tau_l} &= \frac{\pi^2 r_0^2 v_c m^3 N(\log)}{\gamma\Gamma}\left[\frac{\gamma^2}{\sigma_\delta^2}\right]\int_0^\infty \frac{d\lambda\ \lambda^{1/2}\left[a_l\lambda + b_l\right]}{(\lambda^3 + a\lambda^2 + b\lambda + c)^{3/2}}\ , \\
\frac{1}{\tau_y} &= \frac{\pi^2 r_0^2 v_c m^3 N(\log)}{\gamma\Gamma}\left[\frac{\beta_y}{\epsilon_y}\right]\int_0^\infty \frac{d\lambda\ \lambda^{1/2}\left[a_y\lambda + b_y\right]}{(\lambda^3 + a\lambda^2 + b\lambda + c)^{3/2}}\ .
\end{aligned} \tag{8}$$

The coefficients a and b of the denominator are the same for all three planes. The eight coefficients a, b, a_x, b_x, a_l, b_l, a_y, and b_y depend on the approximation. They are listed in Table 1 for all three approaches, i.e., Bjorken-Mtingwa's ultrarelativistic limit, the Conte-Martini formulae, and the expressions including vertical dispersion newly derived. In the limit of vanishing vertical dispersion, the latter (4th column) reduce to the IBS emittance growth rates of Conte and Martini [4] (3rd column).

Table 1: Coefficients for the IBS growth rate expressions, Eq. (8), in the three formalisms. In the limit of zero vertical dispersion, the rightmost column reduces to the Conte-Martini expressions.

	Bjorken-Mtingwa [1]	Conte-Martini [4]	this paper & new MAD-X
a	$\frac{\gamma^2 H_x}{\epsilon_x} + \frac{\gamma^2}{\sigma_\delta^2}$	$\frac{\gamma^2 H_x}{\epsilon_x} + \frac{\gamma^2}{\sigma_\delta^2} + \frac{\beta_x}{\epsilon_x} + \frac{\beta_y}{\epsilon_y}$	$\gamma^2\left(\frac{H_x}{\epsilon_x} + \frac{H_y}{\epsilon_y}\right) + \frac{\gamma^2}{\sigma_\delta^2} + \left(\frac{\beta_x}{\epsilon_x} + \frac{\beta_y}{\epsilon_y}\right)$
b	$\left(\frac{\beta_x}{\epsilon_x} + \frac{\beta_y}{\epsilon_y}\right)\left(\frac{\gamma^2 D_x^2}{\epsilon_x\beta_x} + \frac{\gamma^2}{\sigma_\delta^2}\right)$ $+\frac{\beta_x\beta_y}{\epsilon_x\epsilon_y}\gamma^2\phi_x^2$	$\left(\frac{\beta_x}{\epsilon_x} + \frac{\beta_y}{\epsilon_y}\right)\left(\frac{\gamma^2 D_x^2}{\epsilon_x\beta_x} + \frac{\gamma^2}{\sigma_\delta^2}\right)$ $+\frac{\beta_x\beta_y}{\epsilon_x\epsilon_y}\gamma^2\phi_x^2 + \frac{\beta_x\beta_y}{\epsilon_x\epsilon_y}$	$\left(\frac{\beta_x}{\epsilon_x} + \frac{\beta_y}{\epsilon_y}\right)\left(\frac{\gamma^2 D_x^2}{\epsilon_x\beta_x} + \frac{\gamma^2 D_y^2}{\epsilon_y\beta_y} + \frac{\gamma^2}{\sigma_\delta^2}\right)$ $+\frac{\beta_x\beta_y}{\epsilon_x\epsilon_y}\gamma^2\left(\phi_x^2 + \phi_y^2\right) + \frac{\beta_x\beta_y}{\epsilon_x\epsilon_y}$
c	$\frac{\beta_x\beta_y}{\epsilon_x\epsilon_y}\left(\frac{\gamma^2 D_x^2}{\epsilon_x\beta_x} + \frac{\gamma^2}{\sigma_\delta^2}\right)$	$\frac{\beta_x\beta_y}{\epsilon_x\epsilon_y}\left(\frac{\gamma^2 D_x^2}{\epsilon_x\beta_x} + \frac{\gamma^2}{\sigma_\delta^2}\right)$	$\frac{\beta_x\beta_y}{\epsilon_x\epsilon_y}\left(\frac{\gamma^2 D_x^2}{\epsilon_x\beta_x} + \frac{\gamma^2 D_y^2}{\epsilon_y\beta_y} + \frac{\gamma^2}{\sigma_\delta^2}\right)$
a_x	$\frac{2\gamma^2 H_x}{\epsilon_x} + \frac{2\gamma^2}{\sigma_\delta^2}$	$\frac{2\gamma^2 H_x}{\epsilon_x} + \frac{2\gamma^2}{\sigma_\delta^2} - 2\frac{\beta_x}{\epsilon_x} - \frac{\beta_y}{\epsilon_y}$ $+\frac{\beta_x}{\gamma^2 H_x}\left(\frac{6\beta_x}{\epsilon_x}\gamma^2\phi_x^2\right.$ $\left.-\frac{\gamma^2}{\sigma_\delta^2} + \frac{2\beta_x}{\epsilon_x} - \frac{\beta_y}{\epsilon_y}\right)$	$2\gamma^2\left(\frac{H_x}{\epsilon_x} + \frac{H_y}{\epsilon_y} + \frac{1}{\sigma_\delta^2}\right)$ $-\frac{\beta_x H_y}{H_x\epsilon_y} + \frac{\beta_x}{H_x\gamma^2}\left(\frac{2\beta_x}{\epsilon_x} - \frac{\beta_y}{\epsilon_y} - \frac{\gamma^2}{\sigma_\delta^2}\right)$ $-2\frac{\beta_x}{\epsilon_x} - \frac{\beta_y}{\epsilon_y} + \frac{\beta_x}{\gamma^2 H_x}\left(\frac{6\beta_x}{\epsilon_x}\gamma^2\phi_x^2\right)$
b_x	$\left(\frac{\beta_x}{\epsilon_x} + \frac{\beta_y}{\epsilon_y}\right)\left(\frac{\gamma^2 D_x^2}{\epsilon_x\beta_x} + \frac{\gamma^2}{\sigma_\delta^2}\right)$ $+\frac{\beta_x}{\epsilon_x}\frac{\beta_z}{\epsilon_z}\gamma^2\phi_x^2$	$\left(\frac{\beta_x}{\epsilon_x} + \frac{\beta_y}{\epsilon_y}\right)\left(\frac{\gamma^2 H_x}{\epsilon_x} + \frac{\gamma^2}{\sigma_\delta^2}\right)$ $-\frac{\beta_x^2}{\epsilon_x^2}\gamma^2\phi_x^2 + \left(\frac{\beta_x}{\epsilon_x} - \frac{4\beta_y}{\epsilon_y}\right)\frac{\beta_x}{\epsilon_x}$ $+\frac{\beta_x}{\gamma^2 H_x}\left(\frac{\gamma^2}{\sigma_\delta^2}\left(\frac{\beta_x}{\epsilon_x} - \frac{2\beta_y}{\epsilon_y}\right)\right.$ $\left.+\left\{\frac{\mathbf{6\beta_x\beta_y}}{\mathbf{\epsilon_x\epsilon_y}}\boldsymbol{\gamma^2\phi_x^2}\right\}\right.$ $\left.+\frac{\beta_x\beta_y}{\epsilon_x\epsilon_y} - \gamma^2\frac{\beta_x^2\phi_x^2}{\epsilon_x^2}\right)$	$\left(\frac{\beta_x}{\epsilon_x} + \frac{\beta_y}{\epsilon_y}\right)\left(\frac{\gamma^2 H_x}{\epsilon_x} + \frac{\gamma^2 H_y}{\epsilon_y} + \frac{\gamma^2}{\sigma_\delta^2}\right)$ $-\gamma^2\left(\frac{\beta_x^2}{\epsilon_x^2}\phi_x^2 + \frac{\beta_y^2}{\epsilon_y^2}\phi_y^2\right) + \left(\frac{\beta_x}{\epsilon_x} - \frac{4\beta_y}{\epsilon_y}\right)\frac{\beta_x}{\epsilon_x}$ $+\frac{\beta_x}{\gamma^2 H_x}\left(\frac{\gamma^2}{\sigma_\delta^2}\left(\frac{\beta_x}{\epsilon_x} - \frac{2\beta_y}{\epsilon_y}\right) + \frac{\beta_x\beta_y}{\epsilon_x\epsilon_y}\right.$ $\left.+\frac{6\beta_x\beta_y}{\epsilon_x\epsilon_y}\gamma^2\phi_x^2 + \gamma^2\left(\frac{2\beta_y^2\phi_y^2}{\epsilon_y^2} - \frac{\beta_x^2\phi_x^2}{\epsilon_x^2}\right)\right)$ $+\frac{\beta_x H_y}{\epsilon_y H_x}\left(\frac{\beta_x}{\epsilon_x} - \frac{2\beta_y}{\epsilon_y}\right)$
a_l	$2\gamma^2\left(\frac{H_x}{\epsilon_x} + \frac{1}{\sigma_\delta^2}\right)$	$2\gamma^2\left(\frac{H_x}{\epsilon_x} + \frac{1}{\sigma_\delta^2}\right) - \frac{\beta_x}{\epsilon_x} - \frac{\beta_y}{\epsilon_y}$	$2\gamma^2\left(\frac{H_x}{\epsilon_x} + \frac{H_y}{\epsilon_y} + \frac{1}{\sigma_\delta^2}\right) - \frac{\beta_x}{\epsilon_x} - \frac{\beta_y}{\epsilon_y}$
b_l	$\left(\frac{\beta_x}{\epsilon_x} + \frac{\beta_y}{\epsilon_y}\right)\left(\frac{\gamma^2 D_x^2}{\epsilon_x\beta_x} + \frac{\gamma^2}{\sigma_\delta^2}\right)$ $+\frac{\beta_x\beta_y}{\epsilon_x\epsilon_y}\gamma^2\phi_x^2$	$\left(\frac{\beta_x}{\epsilon_x} + \frac{\beta_y}{\epsilon_y}\right)\left(\frac{\gamma^2 D_x^2}{\epsilon_x\beta_x} + \frac{\gamma^2}{\sigma_\delta^2}\right)$ $+\frac{\beta_x\beta_y}{\epsilon_x\epsilon_y}\gamma^2\phi_x^2 - \frac{2\beta_x\beta_y}{\epsilon_x\epsilon_y}$	$\left(\frac{\beta_x}{\epsilon_x} + \frac{\beta_y}{\epsilon_y}\right)\gamma^2\left(\frac{H_x}{\epsilon_x} + \frac{H_y}{\epsilon_y} + \frac{1}{\sigma_\delta^2}\right)$ $-2\frac{\beta_x\beta_y}{\epsilon_x\epsilon_y} - \gamma^2\left(\frac{\beta_x^2\phi_x^2}{\epsilon_x^2} + \frac{\beta_y^2\phi_y^2}{\epsilon_y^2}\right)$
a_y	$-\frac{\gamma^2 H_x}{\epsilon_x} - \frac{\gamma^2}{\sigma_\delta^2}$	$-\gamma^2\left(\frac{H_x}{\epsilon_x} + \frac{\gamma^2}{\sigma_\delta^2} + \frac{\beta_x}{\epsilon_x} - \frac{2\beta_y}{\epsilon_y}\right)$	$-\gamma^2\left(\frac{H_x}{\epsilon_x} + \frac{2H_y}{\epsilon_y} + \frac{\beta_x}{\beta_y}\frac{H_y}{\epsilon_x} + \frac{1}{\sigma_\delta^2}\right)$ $+2\gamma^4\frac{H_y}{\beta_y}\left(\frac{H_y}{\epsilon_y} + \frac{H_x}{\epsilon_x}\right) + \frac{2\gamma^4 H_y}{\beta_y\sigma_\delta^2}$ $-\left(\frac{\beta_x}{\epsilon_x} - \frac{2\beta_y}{\epsilon_y}\right) + \left(\frac{6\beta_y}{\epsilon_y}\gamma^2\phi_y^2\right)$
b_y	$\left(\frac{\beta_x}{\epsilon_x} + \frac{\beta_y}{\epsilon_y}\right)\left(\frac{\gamma^2 D_x^2}{\epsilon_x\beta_x} + \frac{\gamma^2}{\sigma_\delta^2}\right)$ $+\frac{\beta_x\beta_y}{\epsilon_x\epsilon_y}\gamma^2\phi_x^2$ $-\frac{3\beta_x}{\epsilon_x}\left(\frac{\gamma^2 D_x^2}{\epsilon_x\beta_x} + \frac{\gamma^2}{\sigma_\delta^2}\right)$	$\left(\frac{\beta_x}{\epsilon_x} + \frac{\beta_y}{\epsilon_y}\right)\left(\frac{\gamma^2 D_x^2}{\epsilon_x\beta_x} + \frac{\gamma^2}{\sigma_\delta^2}\right)$ $+\frac{\beta_x\beta_y}{\epsilon_x\epsilon_y}\gamma^2\phi_x^2 + \frac{\beta_x\beta_y}{\epsilon_x\epsilon_y}$ $-\frac{3\beta_x}{\epsilon_x}\left(\frac{\gamma^2 D_x^2}{\epsilon_x\beta_x} + \frac{\gamma^2}{\sigma_\delta^2}\right)$	$\gamma^2\left(\frac{\beta_y}{\epsilon_y} - \frac{2\beta_x}{\epsilon_x}\right)\left(\frac{H_x}{\epsilon_x} + \frac{1}{\sigma_\delta^2}\right)$ $+\left(\frac{\beta_y}{\epsilon_y} - \frac{4\beta_x}{\epsilon_x}\right)\frac{\gamma^2 H_y}{\epsilon_y}$ $+\frac{\beta_x\beta_y}{\epsilon_x\epsilon_y} + \gamma^2\left(\frac{2\beta_x^2\phi_x^2}{\epsilon_x^2} - \frac{\beta_y^2\phi_y^2}{\epsilon_y^2}\right)$ $+\frac{\gamma^4 H_y}{\beta_y}\left(\frac{\beta_x}{\epsilon_x} + \frac{\beta_y}{\epsilon_y}\right)\left(\frac{H_y}{\epsilon_y} + \frac{1}{\sigma_\delta^2}\right)$ $+\left(\frac{\beta_y}{\epsilon_y} + \frac{\beta_x}{\epsilon_x}\right)\gamma^4\frac{H_x H_y}{\beta_y\epsilon_x}$ $-\gamma^4\frac{H_y}{\beta_y}\left(\frac{\beta_x^2}{\epsilon_x^2}\phi_x^2 + \frac{\beta_y^2}{\epsilon_y^2}\phi_y^2\right) + \frac{6\beta_x\beta_y}{\epsilon_x\epsilon_y}\gamma^2\phi_y^2$

4 First Example: LHC

In the LHC, vertical dispersion is generated by the vertical crossing angles at Interaction Points 1 and 2 (and, in the future, possibly also 8), by the spectrometer dipoles together with the detector solenoid fields of ALICE and LHCb, and by the a_2 skew-quadrupole field component in the main dipole magnets. The peak vertical dispersion in the arcs is close to 0.2 m. Figure 1 shows the nominal LHC dispersion at top energy for LHC optics version 6.503. Table 2 lists IBS growth rates computed by the new MAD-X version, which correctly includes the effect of vertical dispersion, considering the nominal value of 1.15×10^{11} protons per bunch, a beam energy of 7 TeV, transverse normalized emittances $\gamma\epsilon_{x,y} = 3.75$ μm, 400-MHz RF voltage of 16 MV, an rms bunch length of 7.42 cm and relative rms momentum spread 1.11×10^{-4}. In the cases with crossing angles and detector fields, the vertical growth time changes from -2.9×10^6 h (damping) to $+5633$ h for the latest MAD-X routine where the effect of vertical dispersion is correctly taken into account. Figure 2 presents the local IBS growth rates around the ring circumference, computed by the new MAD-X version for the LHC with crossing angles and detector fields. The highest vertical and longitudinal growth rates are found in the interaction regions 1 and 5.

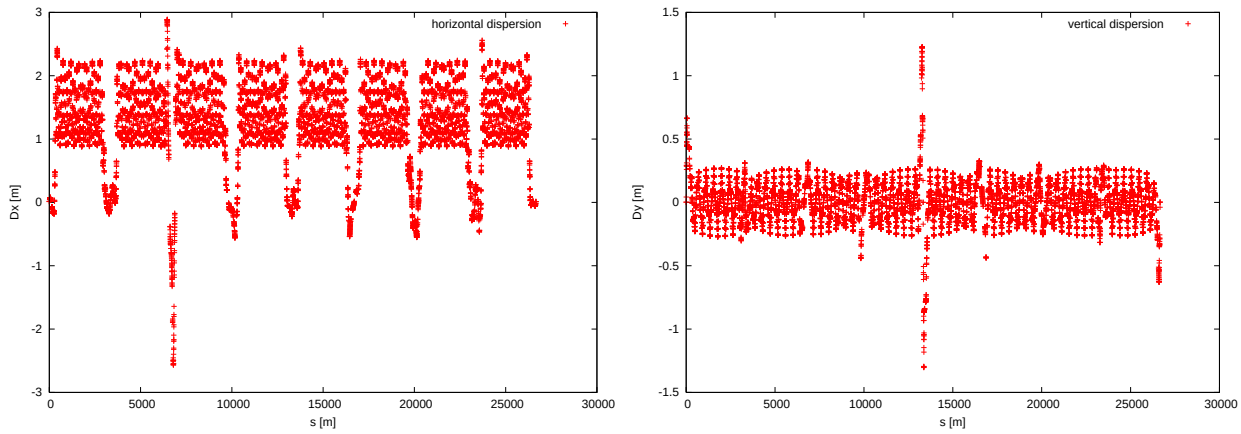

Figure 1: The horizontal (left) and vertical dispersion (right) in units of metre as a function of the position in metre, for the LHC at top energy, with nominal crossing angles and zero separation at IP1, IP2, IP5 and IP8, and the ALICE and LHCb detector fields turned on.

Table 2: LHC IBS growth rates at 7 TeV computed with old (v. 2.0, compiled in 2004) and new versions (v. 5.01, from 2012) of MAD-X with and without crossing angles & LHCb/ALICE detector fields. The full crossing angle in IP1 and IP5 is 285 μrad.

	without crossing angles & detector fields	with crossing angles & detector fields
τ_l [h]	57.2	57.4
τ_x [h]	103.6	102.7
τ_y [h]	-2.9×10^6	5633

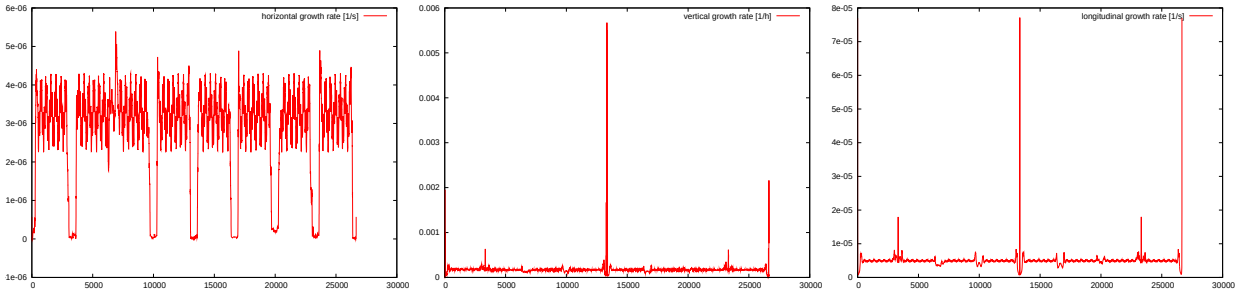

Figure 2: Local horizontal, vertical, and longitudinal IBS growth rates in units of 1/s, 1/h, and 1/s, respectively, as a function of position in m around the ring, for the LHC at top energy, with nominal crossing angles at IP1, IP2, IP5 and IP8, zero separation, and the ALICE and LHCb detector fields turned on.

5 Second Example: LHC Upgrade "ATS" Optics

Upgrades of the LHC are being considered which increase the "virtual peak" luminosity by a factor of twenty to 2×10^{35} cm^{-2}s^{-1}. An essential component of the LHC upgrade plan is a new optics, the so-called ATS optics [11]. We consider the ATS optics "SLHCV3.0" with $\beta^*_{x,y}$ equal to 15 cm in LHC Interaction Points 1 and 5, which would be compatible with the installation and use of crab cavities.

Assuming the ultimate bunch population of 1.7×10^{11} protons, rms normalized transverse emittances of either 2 or 3 μm (this choice of parameter values for emittance and bunch intensity is motivated, e.g., by several presentations at the Chamonix'12 LHC workshop [12]), 400-MHz RF voltages equal to 16 MV and 12 MV, and varying longitudinal emittance, the IBS rates for the nominal LHC optics and the ATS optics are compared in Fig. 3. The IBS rates strongly depend on the bunch length (or longitudinal emittance). For a given bunch length the effect of the RF voltage is rather weak. We also observe that for the ATS optics with $\beta^*_{x,y} = 0.15$ m the transverse IBS rise times are significantly reduced (by factors of about 0.6 and 0.05 in the horizontal and vertical plane, respectively), while the longitudinal rise time is slightly increased (by roughly 20%).

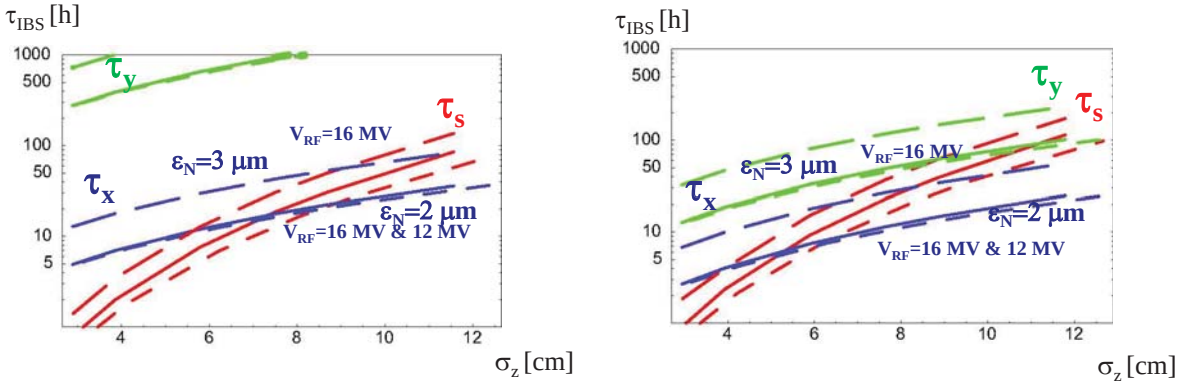

Figure 3: Horizontal, vertical, and longitudinal IBS growth times as a function of rms bunch length for the nominal LHC optics (left) and the ATS optics SLHCV3.0 with 15 cm $\beta^*_{x,y}$ in IPs 1 and 5 (right), considering the ultimate bunch charge, two values of transverse emittance and two different RF voltages, as indicated.

6 Third Example: CLIC Damping Ring

Intrabeam scattering is the dominant effect determining the equilibrium emittance in the CLIC damping rings [13]. Field errors creating vertical dispersion have a profound impact on the estimated vertical growth rate, and, therefore, on the equilibrium emittance. As an illustration, Fig. 4 presents the horizontal and vertical dispersion functions around the CLIC damping ring obtained with random tilt angles of all quadrupole magnets, described by a Gaussian distribution of $\sigma_\phi = 50$ μrad standard deviation with a cut-off at $2.5\sigma_\phi$. One can recognize the two arcs and the two long straight wiggler sections. Table 3 compares the IBS growth rates computed by an old version of MAD-X (2.0), using the Conte-Martini formalism, and those from the new version of the code. While in the case of the ideal optics, there is no difference, the vertical growth time becomes a factor 6 shorter, when errors generating vertical dispersion are included. Figure 5 presents the local IBS growth rates as a function of position around the ring, for the case with errors. The MAD-X results (red solid line) were cross-checked with a direct solution of the Bjorken-Mtingwa equations (1) in Mathematica [14] (blue dashed line), yielding a perfect agreement.

This example underlines that in tuning studies for the CLIC damping ring, the dependence of the IBS growth rate on the residual vertical dispersion must be taken into account.

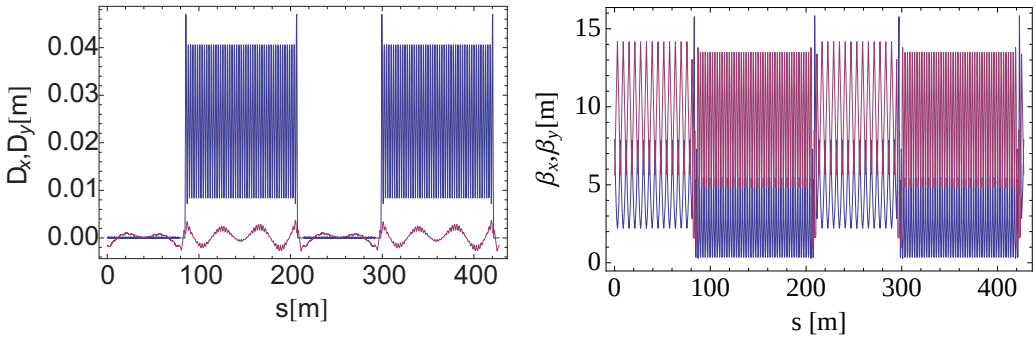

Figure 4: The horizontal and vertical dispersion functions (left) and beta functions (right) in the CLIC damping ring with quadrupole random tilt angles of $\sigma_\phi = 50$ μrad cut off at $2.5\sigma_\phi$.

Table 3: IBS growth rates in the CLIC damping ring computed with old (v. 2.0; compiled in 2004) and new (v. 5.01, from 2012) versions of MAD-X for the ideal optics and with random quadrupole roll angles of $\sigma = 50$ μrad, with a Gaussian distribution cut at 2.5 σ. The following beam parameters are assumed: $\epsilon_x = 5.566 \times 10^{-11}$ m, $\epsilon_x = 5.815 \times 10^{-13}$ m, $\sigma_\delta = 1.21 \times 10^{-3}$, $\sigma_z = 1.461$ mm, and $N = 4.07 \times 10^9$.

	no errors		errors	
	old MAD-X	new MAD-X	old MAD-X	new MAD-X
τ_l [ms]	3.043	2.989	3.043	3.071
τ_x [ms]	0.871	0.855	0.871	0.880
τ_y [ms]	5.577	5.477	5.577	1.426

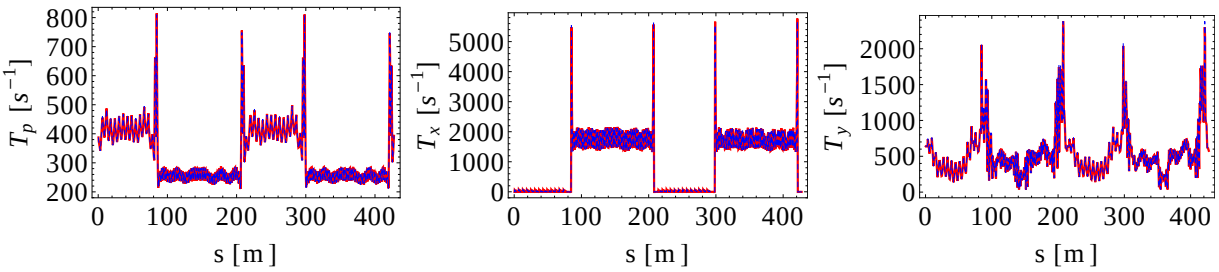

Figure 5: Local longitudinal, horizontal and vertical IBS growth rate in units of 1/s as a function of position in m around the CLIC damping ring, with quadrupole random tilt angles of $\sigma_\phi = 50$ μrad cut off at $2.5\sigma_\phi$. The red solid lines show the growth rates calculated by MAD-X, the blue dashed lines the growth rates those obtained from a direct solution of the fundamental B-M equations (1) in Mathematica.

7 Fourth Example: The SLS model

Ths Swiss Light Source (SLS) storage ring has so far achieved a vertical emittance of 1.9 pm-rad at 2.411 GeV, which is dominated by machine imperfections. In view of the SLS ability to achieve ultra-low vertical emittance, or its possible operation at lower energies, and the availability of suitable emittance monitoring diagnostics, the SLS is an ideal testbed for IBS studies [15].

Figure 6 presents the horizontal and vertical dispersion functions around the SLS obtained with random tilt angles of all quadrupole magnets, described by a Gaussian distribution of $\sigma_\phi = 58$ μrad standard deviation with a cut-off at $2.5\sigma_\phi$, producing a vertical emittance of 2 pm-rad. Table 4 compares the IBS growth rates computed by the new version of the code in the case of the ideal optics and when errors generating vertical dispersion are included. Even in this example where the IBS effect is weak, there is a factor of 7 difference in the vertical growth rate if the vertical dispersion is not taken into account. Figure 7 presents the local IBS growth rates as a function of position around the ring, using the same color convention as in Figure 5.

Table 4: IBS growth rates in the SLS model computed with the correct(ed) version of MAD-X for the ideal optics and with random quadrupole roll angles of $\sigma_\phi = 58$ μrad, with a Gaussian distribution cut at $2.5\sigma_\phi$.

	w/o errors	with errors
τ_l [ms]	12.99	13.99
τ_x [ms]	47.22	49.16
τ_y [ms]	193.14	25.99

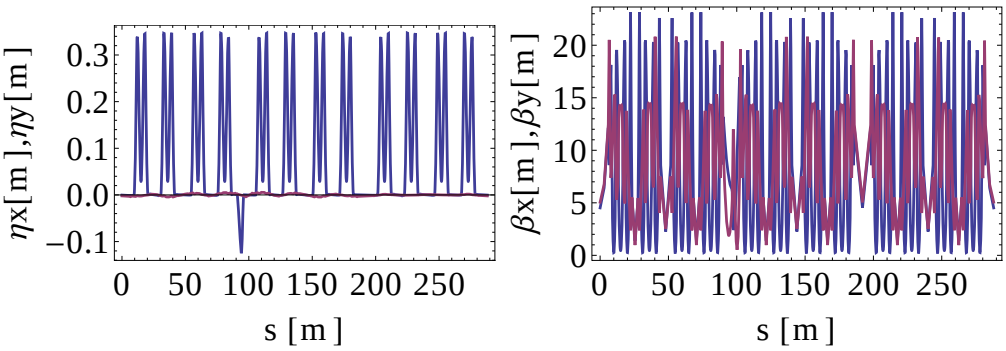

Figure 6: The horizontal and vertical dispersion functions (left) and beta functions (right) in the SLS model with quadrupole random tilt angles of $\sigma_\phi = 58$ μrad cut off at $2.5\sigma_\phi$.

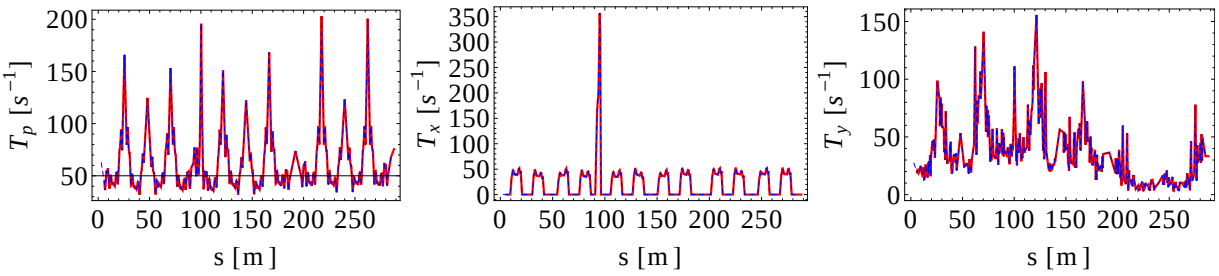

Figure 7: Local longitudinal, horizontal and vertical IBS growth rate in units of 1/s as a function of position in m around the SLS, with quadrupole random tilt angles of $\sigma_\phi = 58\ \mu$rad cut off at $2.5\sigma_\phi$. The blue solid lines show the growth rates calculated by MAD-X, the red dashed lines the growth rates those obtained from a direct solution of the fundamental B-M equations (1) in Mathematica.

8 Limitations and Outlook

The theory of Bjorken-Mtingwa calculates the rms emittance growth rates assuming Gaussian beams. In reality, a beam will not be exactly of Gaussian shape, e.g., due to the effect of intrabeam scattering. The existing theories of Bjorken-Mtingwa or Piwinski do not predict the emittance growth for non-Gaussian distributions, neither do they describe the tails generated by intrabeam scattering.

An attempt to more correctly estimate the emittance growth of the beam core due to intrabeam scattering for electron or positron storage rings was proposed by Raubenheimer [16], who adjusted the upper limit of the Coulomb integral so as to discard single-scattering events over a radiation damping time, thereby removing the contribution of the tail increase to the rms growth rate. This modification reduces the effective growth rate by about a factor of 0.6, compared with the conventional calculation.

An alternative and more comprehensive approach to address and to model tails are multi-particle Monte-Carlo simulations à la MOCAC [17], which is based on a binary collision model [18]. This type of code can model any distribution, but long computing times are implied. We consider adding a Monte-Carlo simulation IBS module to MAD-X in the longer-term future.

Coupling between the horizontal and vertical betatron motion is not accounted for in the formalism presented here.

Lastly, both the Bjorken-Mtingwa paper and our derivation in this paper start from an invariant Coulomb scattering amplitude of the form $M = 4\pi\alpha/q^2$, where α denotes the fine-structure constant and q the four-momentum transfer. This scattering amplitude describes the Coulomb interaction of two charged spinless and point-like particles, with all the entailed limitations.

9 Summary

Applying the Bjorken-Mtingwa formalism, we have derived generalized expressions for the three intrabeam scattering growth rates, which are valid also if the beam energy is not ultrarelativistic, or if vertical dispersion is present either by design or due to errors. In the limit of zero vertical dispersion our result reduces to that of Conte and Martini.

Four examples, from the LHC, the LHC upgrade, the CLIC damping ring and the SLS storage ring respectively, demonstrate that the effect of the vertical dispersion is predominant for the vertical growth rate, which is changed, for the LHC, by four orders of magnitude and in the sign, for the CLIC damping ring with errors, by a factor of 6 and for the SLS storage ring with errors, by a factor of 7. The new IBS formulae have been committed to the MAD-X code [5].

Acknowledgements

We thank A. Bolshakov, O. Brüning, L. Deniau, M. Giovannozzi, J. Jowett, M. Martini, S. Nagaitsev, A. Smirnov, and A. Xiao for helpful discussions, Y. Papaphilippou for important comments and, especially, for proposing the joint investigation of the two authors, M. Korostelev for contributing an earlier optics of the CLIC damping ring, A. Streun for providing the optics of the SLS storage ring and A. Lehrach for re-emphasizing the importance of non-Gaussian distributions at the 2005 MAD-X day. In particular, we are grateful to F. Schmidt for encouraging this study and for his strong support.

[5] The changes are effective starting with MAD-X production version no. 5.01.00, and MAD-X development version no. 5.00.12.

References

[1] J.D. Bjorken, S.K. Mtingwa, “Intrabeam Scattering,” Part. Acc. Vol. 13, pp. 115–143 (1983).

[2] F. Zimmermann, “Intrabeam Scattering with Non-Ultrarelativistic Corrections and Vertical Dispersion for MAD-X,” CERN-AB-2006-002 (2006).

[3] J.Y. Hemery, unpublished; private communication by M. Martini (2005).

[4] M. Conte, M. Martini, “Intrabeam Scatering in the CERN Antiproton Accumulator,” Part. Acc. Vol. 17, pp. 1–10 (1985).

[5] M. Zisman, S. Chattopadhyay, J. Bisognano, ZAP User’s Manual, LBL-21270, ESG-15 (1986).

[6] A. Piwinski, “Intrabeam Scattering,” Proc. Ninth Int. Conference on high Energy Accelerators, Stanford, Springfield, pp. 405–409 (1975).

[7] K.L.F. Bane, “A Simplified Model of Intrabeam Scattering,” EPAC’02 Paris (2002).

[8] M. Martini, private communication, 27 January 2009

[9] A. Xiao (FNAL), private communication, 14 April 2008

[10] K. Kubo, K. Oide, “Intrabeam Scattering in Electron Storage Rings,” PRST-AB 4, 124401 (2001).

[11] S. Fartoukh, “Breaching the Phase I Optics Limitaitons for the HL-LHC,” sLHC Project Report 0053 (2011).

[12] T. Steerenberg, “Performance Reach of the Injector Complex;” H. Damerau, “Performance Potential of the Injectors after LS1;” W. Herr, “Performance Reach of LHC after LS1;” O. Brüning, ‘”HL-LHC Operation with Protons and Ions;” presentations at the LHC Performance Workshop 2012, Chamonix, 6–10 February 2012

[13] F. Antoniou, M. Martini, Y. Papaphilippou, A. Vivoli, “Parameter scan for the CLIC Damping Rings under the influence of intrabeam scattering,” IPAC 2010, CERN-ATS-2010-048 and CLIC-Note-833.

[14] F. Antoniou, “Optics Design Optimization for IBS Dominated Beams,” PhD thesis, to be published.

[15] N. Milas et al, “Report on existing hardware limitations and needed upgrades of the storage ring of the Swiss Light Source,” TIARA-REP-WP6-2011-004.

[16] T. Raubenheimer, “The Core Emittance with Intrabeam Scattering in e+/e- Storage Rings,” Part. Acc. 45, 111 (1994).

[17] P. Zenkevich, A. Bolshakov, O. Boine-Frankenheim, “Kinetic Effects in Multiple Intra-Beam Scattering,” ICFA HB204, Bensheim, AIP Conf. Proc. 773, 425 (2005).

[18] T. Takizuka and H. Abe, “A Binary Collision Model for Plasma Simulation with a Particle Code,” J. Comp. Physics 25, pp. 205–219 (1977).